Investigation of film surface roughness and porosity dependence on lattice size in a porous thin film deposition process

Gangshi Hu, Jianqiao Huang, Gerassimos Orkoulas, and Panagiotis D. Christofides*
Department of Chemical and Biomolecular Engineering, University of California, Los Angeles, California 90095, USA
(Received 30 June 2009; published 21 October 2009)

The dependence of film surface roughness and porosity on lattice size in a porous thin film deposition process is studied via kinetic Monte Carlo simulations on a triangular lattice. For sufficiently large lattice size the steady-state value of the expected film porosity has a weak dependence on the lattice size and the steady-state value of the expected surface roughness square varies linearly with lattice size. An analysis of the film morphology based on a stochastic partial differential equation description of the film surface morphology supports and explains the findings of the numerical simulations.

DOI: 10.1103/PhysRevE.80.041122 PACS number(s): 02.50.Ng, 05.10.Ln, 02.50.Ey, 05.10.Gg

I. INTRODUCTION

Thin film growth processes are significant in many areas, e.g., manufacturing of microelectronic devices and solar cells. To understand the mechanisms and further improve the operating conditions and yield, extensive research work has focused on the study of thin film growth processes via both experiments and simulations.

Many research efforts on modeling and control of thin film surface roughness focus on the microscopic thin film growth models which utilize a square lattice with solid-on-solid (SOS) approximation that excludes vacancies and overhangs from the film microstructure [1]. The SOS models for thin film deposition processes are effective in the development of a methodology to describe the evolution of film microstructure and design feedback control laws for thin film surface roughness [2,3]. However, SOS models are incapable of capturing the evolution of film porosity since vacancies and overhangs are forbidden in the SOS models. In previous work, triangular lattice models that allow for vacancies and overhangs inside the film were introduced to simulate the evolution of porous thin films [4–7] and design model predictive controllers to regulate the film porosity, surface roughness, and/or film thickness [8,9].

Stochastic differential equation (SDE) models are continuum models that can be derived from the thin film growth processes to describe the evolution of thin film morphologies [10–13]. The SDE models contain the morphology information of the thin films and account for the stochastic nature of the microscopic processes. Methodologies have been developed to construct the SDE models and estimate the parameters from first principles [13–15] and numerical simulations [16].

Due to limitations of the currently available computing power, numerical simulations utilize small system sizes and thus cannot access realistic wafer dimensions. However, simulation results on systems of finite (and small) size provide insights to the growth processes and evolution of film microstructure. The dependence of film morphology on system size has attracted many research efforts, both numerically and theoretically [10,17,18]. However, most studies of lattice size dependence focus on the surface height evolution of SOS models [17] or ballistic deposition models [19–21]. The investigation of lattice size dependence for triangular lattice models of porous thin films that involve a thermal balance between adsorption and migration processes has received limited attention.

Motivated by these considerations, this work focuses on the study of the dependence of film surface roughness and porosity on lattice size in a porous thin film deposition process. Specifically, a porous thin film deposition process which includes atom adsorption and migration is considered and is modeled via kinetic Monte Carlo (kMC) simulation on a one-dimensional triangular lattice. Extensive numerical simulations are carried out to determine the variation in the film surface roughness and porosity with lattice size. For sufficiently large lattice size, the steady-state value of the expected film porosity has a weak dependence on the lattice size and the steady-state value of the expected surface roughness square varies linearly with lattice size. A theoretical analysis based on stochastic partial differential equation (PDE) descriptions of the film surface morphology is carried out to support and explain the computational findings.

II. PROCESS DESCRIPTION AND DEFINITIONS OF VARIABLES

In this section, a thin film deposition process is modeled and simulated by using an on-lattice kinetic Monte Carlo model, which allows vacancies and overhangs to develop inside the film. Definitions of film site occupancy ratio and film surface roughness are introduced for the convenience of discussions on the lattice size dependence in later sections.

A. On-lattice kinetic Monte Carlo model of deposition process

The thin film deposition process considered in this work is modeled on a two-dimensional triangular lattice (one dimension on the growth direction) via kMC methods; see Fig. 1 [9]. In the simulation of the deposition process, it is as-

*Also at Department of Electrical Engineering, University of California, Los Angeles, CA 90095, USA. FAX: +1(310)206-4107; pdc@seas.ucla.edu

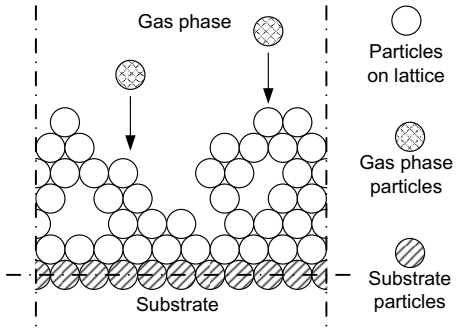

FIG. 1. Thin film growth process on a triangular lattice.

sumed that all particles occupy discrete lattice sites. This assumption is valid for low temperatures, $T<0.5T_m$, where T_m is the melting point of the crystal [4]. The lattice size is the number of sites in the direction perpendicular to the growth direction (i.e., the horizontal direction, see Fig. 1). The number of nearest neighbors of a site ranges from zero to six, the coordination number of the triangular lattice. In the lattice, a bottom layer acts as the substrate for the deposition process. The substrate layer is initially set to be fully packed and fixed, as shown in Fig. 1.

Two types of microscopic processes (Monte Carlo events in the kMC simulation) are considered: an adsorption process, in which particles are incorporated into the film from the gas phase, and a migration process, in which particles move to their adjacent sites [4,6,7,22]. The microstructure of the thin film is the result of the complex interaction between the two microscopic processes. The macroscopic parameters that influence the deposition process are the adsorption rate, W, and the substrate temperature, T. Both the adsorption rate and the substrate temperature are assumed to be uniform throughout the film and are treated as time varying but spatially invariant process parameters. The incident angle (including its probability distribution) is another important process parameter that affects the deposition process. Only the vertical incidence is considered in this work to minimize the non-local shadowing effect [9]. A brief description of the adsorption and migration processes is given below.

In an adsorption process, a particle from the gas phase comes in contact with the film and is incorporated onto the film. The macroscopic adsorption rate, W, is defined as the

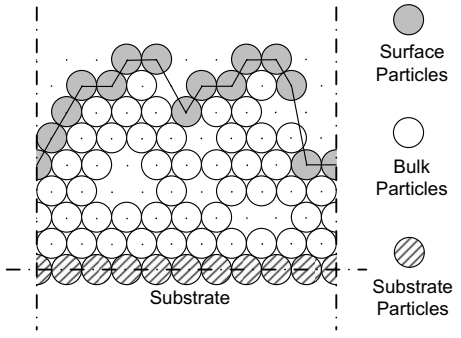

FIG. 2. Definition of surface height profile. A surface particle is a particle that is not blocked by particles from both of its neighboring columns in the vertical direction.

number of deposited layers per second. A particle is initially placed at a random position above the thin film, as shown in Fig. 1. After the initial position is determined, the incident particle travels vertically toward the film and sticks to the first particle on the film that it contacts. The incident particle then moves to the nearest vacant site and is subject to instantaneous surface relaxation if the new site is unstable, i.e., the new site has only one neighboring particle [9]. When a particle is subject to surface relaxation, the particle moves to its most stable neighboring vacant site, which is defined as the site with the most nearest neighbors. In the case of multiple neighboring vacant sites with the same number of nearest neighbors, a random one is chosen from these sites with equal probability. Note that particle surface relaxation is considered as part of the deposition event, and thus, it does not contribute to the process simulation time. There is at most one relaxation event per incident particle.

In a migration process, a particle overcomes the energy barrier of the site and jumps to its vacant neighboring site with a migration rate (probability) that depends on its local environment (i.e., the number of nearest neighbors) and the substrate temperature. The migration rate follows an Arrhenius-type law:

$$r_{m,i} = \nu_0 \exp\left(-\frac{n_i E_0}{k_B T}\right), \tag{1}$$

where ν_0 is a pre-exponential factor, $n_i=1$, 2, 3, 4, and 5, is the number of the nearest neighbors of the ith particle, E_0 is the contribution to the activation energy barrier from each nearest neighbor and k_B is the Boltzmann's constant. The diffusion rate is zero when $n_i=6$ since this particle is fully surrounded by other particles and cannot migrate. When a particle is subject to migration, it can jump to either of its vacant neighboring sites that have at least one nearest neighbor with equal probability. Particles cannot migrate to vacant neighboring sites that have no nearest neighbors.

In this work, the continuous-time Monte Carlo (CTMC) method [23] is used in the kMC simulations of the thin film deposition process due to its high efficiency in simulations of rare events. According to the CTMC algorithm, a list of events is constructed and an event is selected randomly with its respective probability. After the execution of the selected event, the list is updated based on the new lattice structure. The computational efficiency of the kMC simulation is further improved by utilizing a grouping algorithm [24] to speed up the selection process of the particle that is subject to a migration process.

Determination of the migration rate requires specification of the parameters ν_0 and E_0 in Eq. (1). In this work, we select $\nu_0=10^{13}$ s^{-1} and $E_0=0.6$ eV that are appropriate for a silicon film [25].

B. Definitions of surface roughness and film site occupancy ratio

Following our previous work [9], the film microstructure is described by two variables: surface roughness and film porosity, respectively. Surface roughness is a measure of thin film surface texture and is represented by the root mean

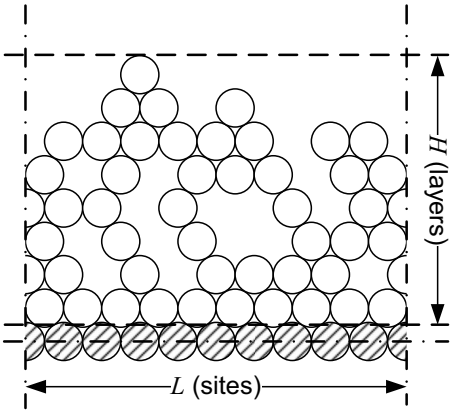

FIG. 3. Illustration of the definition of film site occupancy ratio (SOR) of Eq. (3).

square (rms) of the surface height profile of the thin film. The profile of the surface height is found by connecting the sites that are occupied by surface particles; see Fig. 2. Surface particles are the particles that are not blocked by particles in both neighboring columns and can be reached in the vertical direction, as shown in Fig. 2. Surface roughness, r, is defined as the standard deviation of the surface height profile from its average height as follows [9]:

$$r = \sqrt{\frac{1}{L}\sum_{i=1}^{L}(h_i - \bar{h})^2}, \tag{2}$$

where $\bar{h} = \frac{1}{L}\sum_{i=1}^{L} h_i$ is the average surface height. Note that $r \geq 0$ and $r=0$ corresponds to a flat surface.

Film site occupancy ratio (SOR) measures the porosity of the thin film and is defined as the fraction of sites that are occupied by particles as follows [8,9]:

$$\rho = \frac{N}{LH}, \tag{3}$$

where ρ denotes the film SOR, N is the total number of deposited particles on the lattice, L is the lattice size, and H is the number of deposited layers; see Fig. 3. Note that the deposited layers are the layers that contain only deposited particles and do not include the initial substrate layers. Since each layer contains L sites, the total number of available sites in the H layers is LH. Thus, film SOR is the ratio of the occupied lattice sites, N, over the total number of available sites, LH. With this definition, film SOR ranges from 0 to 1. Specifically, $\rho=1$ denotes a fully occupied film. The value of zero is assigned to ρ at the beginning of the deposition process since there are no particles deposited on the lattice.

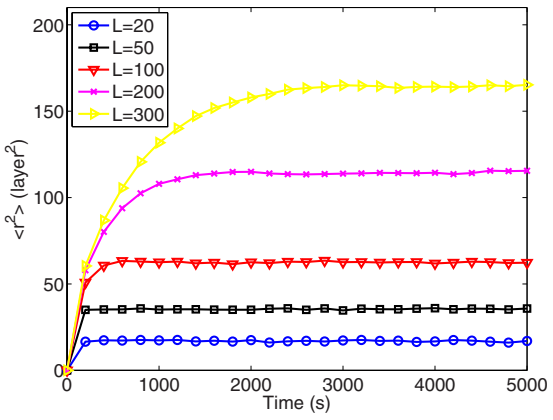

FIG. 4. (Color online) Profiles of the expected surface roughness square from kMC simulations with different lattice sizes; $W=1$ layer/s and $T=300$ K.

TABLE I. Number of simulation runs (surface roughness) for different lattice sizes.

L	$T=300$ K	$T=400$ K	$T=500$ K
20	5000	5000	5000
50	5000	5000	5000
100	5000	5000	5000
200	20000	15000	10000
300	20000	15000	15000
400	15000		
500	15000		

The two film properties, film surface roughness and SOR, are not independent. The main reason for which surface roughness and SOR are coupled is that they are both affected by the adsorption and migration processes in a similar fashion. At high temperature or low adsorption rate, the relatively stronger influence of migration process tends to produce a denser and smoother film with less holes and thus it results in a higher SOR and a smaller roughness; and vice versa. Moreover, the layers containing the rough surface are newly deposited and have not experienced enough time for migration. Thus, these layers generally have higher porosity than the layers in the bulk film. According to the definition of film SOR of Eq. (3) and the illustration of film SOR of Fig. 3, all layers below the top layer (including the more porous layers that contain the rough surface) are counted for the calculation of film SOR. In this way, surface roughness contributes to film SOR. This contribution is significant at the beginning of film growth, since the film thickness is relatively small. However, at large times, the film thickness is sufficiently large, and thus, the contribution from a rough surface to the SOR is negligible. Different definitions of surface roughness and porosity may be used but do not affect the main conclusions in this work, especially at large times.

Due to the stochastic nature of microscopic processes, a profile from a single simulation cannot give meaningful results. Therefore, the expected values of the film surface roughness and SOR are obtained as averages over multiple independent simulations. The specific numbers of simulation runs depend on the operating conditions, as it will be explained below.

III. LATTICE SIZE DEPENDENCE OF SURFACE ROUGHNESS

In this section, the dependence of film surface roughness on lattice size is investigated via numerical simulations and

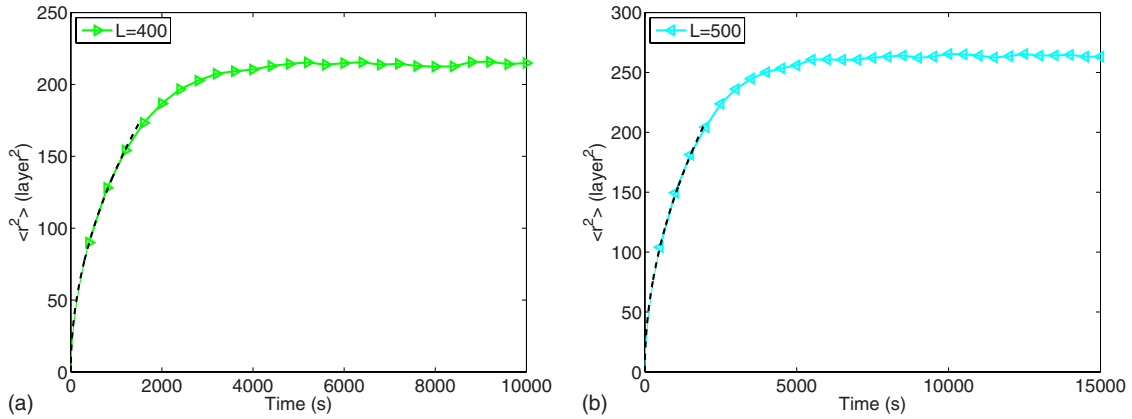

FIG. 5. (Color online) Profiles of the expected surface roughness square from kMC simulations (solid lines) and the fitted power-law time dependence with an exponent of 0.5 for short times ($\langle r^2\rangle = r_0\sqrt{t}$, dashed lines), with different lattice sizes (a) $L=400$ and (b) $L=500$; $W=1$ layer/s and $T=300$ K.

theoretical methods that are based on stochastic partial differential equation models for the evolution of the surface height profile.

A. Computational results from the kinetic Monte Carlo model

To investigate the dependence of surface roughness on the lattice size, kMC simulations of the thin film deposition process with different lattice sizes are carried out. The substrate temperature and the adsorption rate are kept fixed throughout the entire simulation. The simulation time is set to be sufficiently long so that the profile of surface roughness has reached the steady-state regime. Simulation results are averaged from multiple independent simulation runs (5000–20 000) to obtain smooth profiles. The specific numbers of independent simulation runs are listed in Table I.

Figure 4 shows the profiles of the expected surface roughness square with different lattice sizes (from 20 to 300) at an adsorption rate of 1 layer/s and a substrate temperature of 300 K. The profiles of the two larger lattice sizes, $L=400$ and 500, are shown in Fig. 5 since it takes longer time to reach the steady state. From Figs. 4 and 5, it can been seen that, regardless of the lattice size, the expected surface roughness square increases from zero and finally reaches a steady-state value at large times. Figures 5 and 6 also show that the increase in the roughness square follows a power law on time with an exponent of 0.5, which indicates $\langle r^2\rangle = r_0\sqrt{t}$, at short times. Figures 4 and 5 further show that as L increases, the time required to reach the steady-state regime also increases.

Analysis of the simulation data indicates that the dependence of surface roughness dynamics on the lattice size is quasiquadratic; see Fig. 7 for the lattice size dependence of the saturation time of the roughness square profiles for $T=300$ K, where the saturation time of the roughness square, $T^{sat}_{\langle r^2\rangle}$, is defined as the time required for the expected surface roughness square to reach very close to its steady-state value. To reduce the influence of the fluctuation, $T^{sat}_{\langle r^2\rangle}$ is obtained from the average of the time instants when the expected roughness square reaches 98.0%, 98.5%, 99.0%, and 99.5% of the steady-state value. From Fig. 7, it can be seen that the saturation time is proportional to the square of the lattice size for $T=300$ K. This quadratic dependence of the dynamics on the lattice size significantly limits the range of lattice sizes that can be studied since a large lattice-size system ($L>500$) may require a much longer time ($t>10\,000$ s) to achieve steady state. Such computational requirements are beyond our current available computing power. However, the range of lattice size that can be studied is sufficient to demonstrate the dependence of surface roughness on the lattice size.

The steady-state values of the expected surface roughness square also exhibit strong dependence on the lattice size. This dependence can be better addressed by plotting the steady-state values, $\langle r^2\rangle_{ss}$, with respect to lattice size; see Fig. 8. The error bars in Fig. 8 represent the range $\langle r^2\rangle_{ss} \pm \sigma_r$, where σ_r denotes the standard deviation of $\langle r^2\rangle_{ss}$ and is calculated from 10 averages of evenly divided groups of all simulation runs. The steady-state values of the expected surface roughness square are determined from the evolution

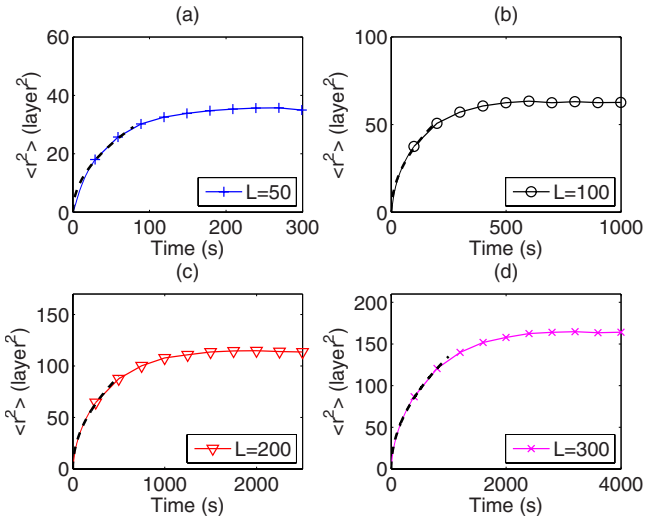

FIG. 6. (Color online) Profiles of the expected surface roughness square from kMC simulations (solid lines) and the fitted power-law time dependence with an exponent of 0.5 for short times ($\langle r^2\rangle = r_0\sqrt{t}$, dashed lines), with different lattice sizes (a) $L=50$, (b) $L=100$, (c) $L=200$, and (d) $L=300$; $W=1$ layer/s and $T=300$ K.

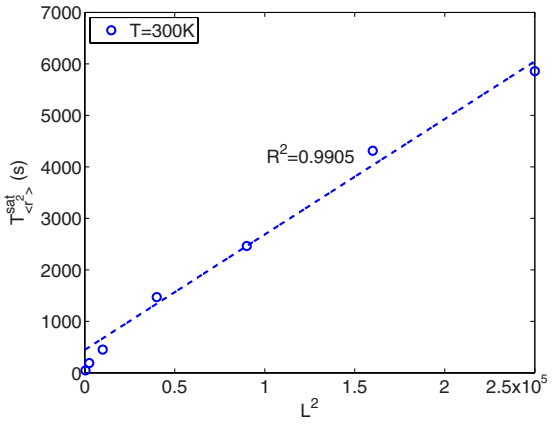

FIG. 7. (Color online) Dependence of the saturation time of the expected surface roughness square, $T^{sat}_{\langle r^2\rangle}$, (symbols) on the lattice size square, and the quadratic regression, $T^{sat}_{\langle r^2\rangle}=kL^2+b$, of the points corresponding to $L\geq 100$ (line); $W=1$ layer/s and $T=300$ K.

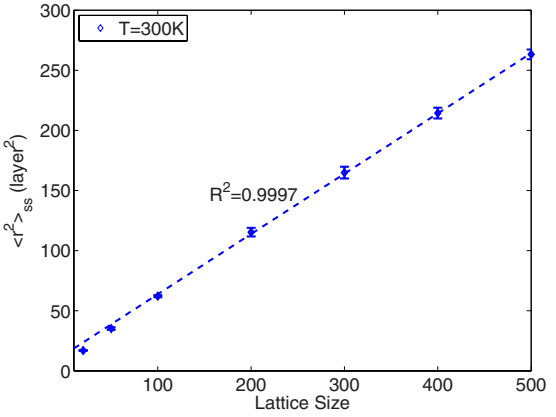

FIG. 8. (Color online) Dependence of the steady-state values of the expected surface roughness square, $\langle r^2\rangle_{ss}$, (symbols with error bars) on the lattice size, and the linear regression, $\langle r^2\rangle_{ss}=k'L+b'$, of the points corresponding to $L\geq 100$ (dashed line); $W=1$ layer/s and $T=300$ K.

profiles of Figs. 4 and 5 by averaging over the last 1000 points where steady state has been clearly reached. A linear dependence on the lattice size is clearly shown in Fig. 8 for large lattice sizes, where the linear regression is obtained from the data points of lattice sizes $L\geq 100$ and the regression coefficient is 0.9997.

The numerical findings from the kMC model at $T=300$ K, e.g., the quadratic dependence of $T^{sat}_{\langle r^2\rangle}$ on lattice size, the linear dependence of $\langle r^2\rangle_{ss}$ on lattice size, and the power-law dependence with 0.5 exponent of roughness square on time for short times, are in accord with the predictions of the Edwards-Wilkinson (EW) equation, which is valid for large lattice sizes ($L\rightarrow\infty$). The detailed derivation is given in Sec. III C later.

B. Influence of substrate temperature on surface roughness

Simulations under different operating conditions are also carried out. According to the Arrhenius-type law of Eq. (1), the substrate temperature, T, may affect the intensity of the migration process, which in turn results in a different evolution of the thin film growth process. Figure 9 shows the evolution profiles of $\langle r^2\rangle_{ss}$ with lattice size at substrate temperatures $T=400$ and 500 K. The adsorption rate is $W=1$ layer/s for all simulations. Although different substrate temperatures may result in different dynamics and steady-state values, the lattice-size dependence of the saturation time and of the steady-state value, shown in Figs. 10 and 11, is still quadratic and linear, respectively, as it was at $T=300$ K.

To further understand the influence of substrate temperature on surface roughness, a series of kMC simulations was carried out at different temperatures. Figure 12 shows the profiles of the expected surface roughness square at different substrate temperatures. A lattice size of 100 sites is used in all simulations of Fig. 12 for a meaningful comparison. Dependence of the steady-state surface roughness square on the substrate temperature is shown in Fig. 13. It can be clearly seen from Fig. 13 that the substrate temperature has a strong influence on the evolution of surface roughness. Figures 14 and 15 show, respectively, the snapshots of film microstructure and surface morphology of thin films at the end of the simulations ($t=5000$ s) with different substrate temperatures.

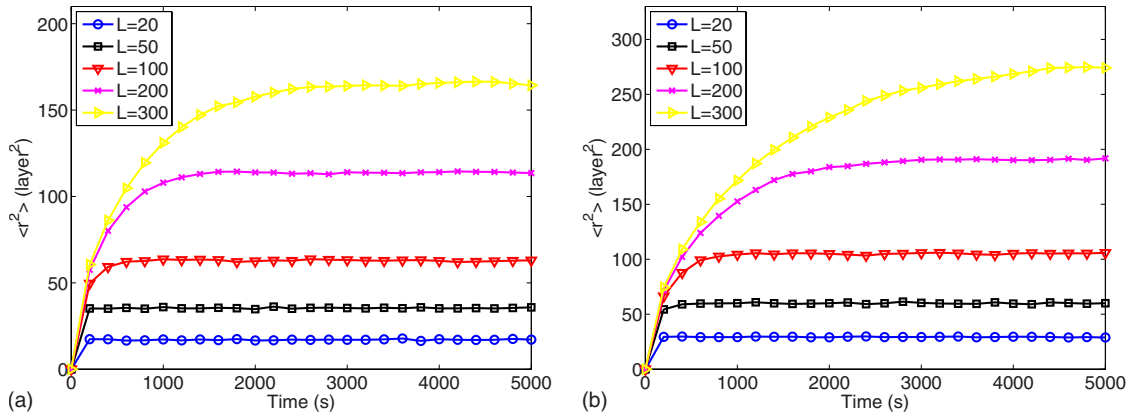

FIG. 9. (Color online) Profiles of the expected surface roughness square from kMC simulations with different lattice sizes at (a) $T=400$ K and (b) $T=500$ K; $W=1$ layer/s.

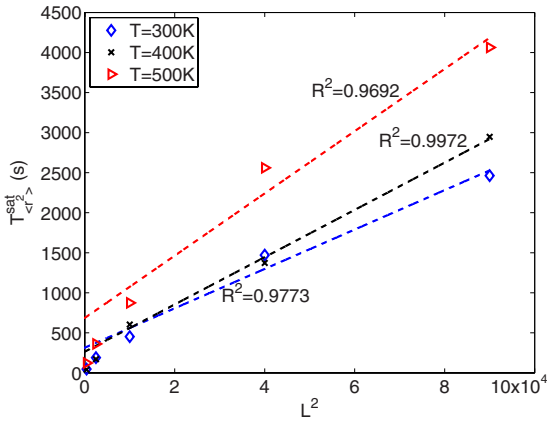

FIG. 10. (Color online) Dependence of the saturation time of the expected surface roughness square, $T^{sat}_{\langle r^2\rangle}$, (symbols) on the lattice size square, and the quadratic regression, $T^{sat}_{\langle r^2\rangle}=kL^2+b$, of the points corresponding to $L\geq 100$ (lines), at different substrate temperatures; $W=1$ layer/s.

At low temperatures ($T\leq 400$ K), it can be seen from Fig. 14 that a porous microstructure is formed in the thin film, which is due to the lack of particle mobility owing to the very small particle migration rates relative to the adsorption rate. As a result, surface roughness profiles are insensitive to the substrate temperature. As the temperature increases above 400 K, the thin film microstructure evolves differently. Specifically, the increased particle mobility (migration) at higher temperatures results in higher numbers of nearest neighbors, which lowers the film porosity and results in a denser film and smaller film thickness; see Fig. 14. Also, this aggregation of surface particles first leads to a grainy surface morphology and a higher surface roughness; see Fig. 15. Thus, it can be seen from Fig. 13 that the steady-state values of the expected surface roughness square increase and reach a maximum at around 600 K. When the temperature further increases above 600 K, however, the steady-state values of the expected surface roughness square start decreasing. This is due to the domination of the migration process,

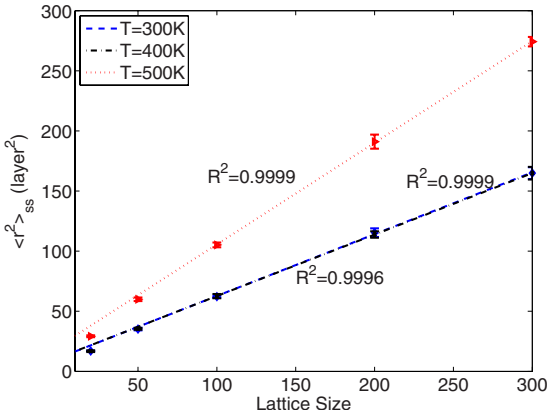

FIG. 11. (Color online) Dependence of the steady-state values of the expected surface roughness square, $\langle r^2\rangle_{ss}$, (symbols with error bars) on the lattice size, and the linear regression, $\langle r^2\rangle_{ss}=k'L+b'$, of the points corresponding to $L\geq 100$ (lines), at different substrate temperatures; $W=1$ layer/s.

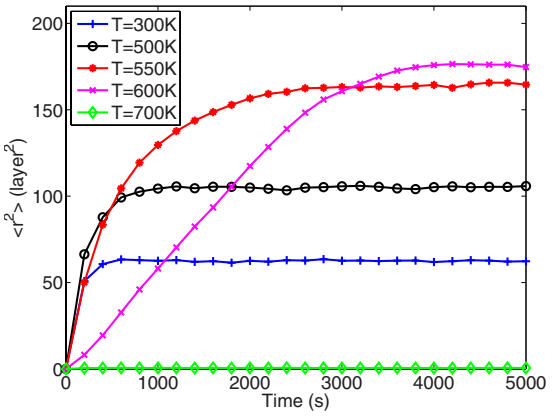

FIG. 12. (Color online) Profiles of the expected surface roughness square at different substrate temperatures; $W=1$ layer/s and $L=100$.

which tends to smooth the film surface. Ultimately, at high temperatures ($T\geq 700$ K), the film surface is flat with the expected surface roughness approaching zero. Furthermore, for $T\geq 700$ K, the film body is almost fully packed with very little porosity. The flat surface and the dense film at high temperatures can be also seen in the surface morphology in Fig. 15 and in the film microstructure in Fig. 14, respectively. Please note that even the high temperature limit used in the simulations, $T=700$ K, is still within the valid range of temperature for an on-lattice kMC model ($T\leq T_m/2=844$ K for a silicon film).

Remark 1. Similar to the substrate temperature, another process parameter, the adsorption rate, also influences the deposition process and the evolution of surface roughness. Different adsorption rates result in different balances between the adsorption process and the migration process. In general, a higher adsorption rate may enhance the thin film growth but result in higher surface roughness and porosity. Such influences are similar to the ones induced by a lower substrate temperature. Therefore, the influence of the adsorption rate can be inferred from the results of the substrate temperature and is not included here.

Remark 2. The initial dynamics of the expect surface

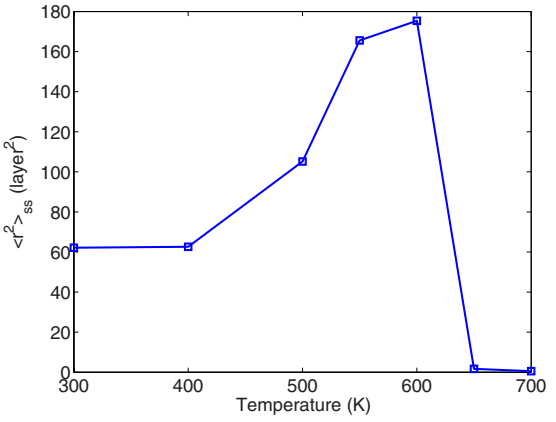

FIG. 13. (Color online) Dependence of the steady-state values of the expected surface roughness square on the substrate temperature; $W=1$ layer/s and $L=100$.

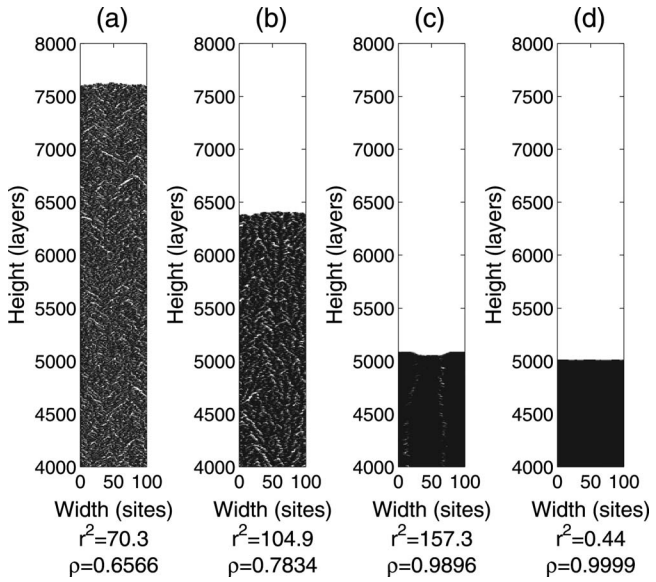

FIG. 14. Snapshots of film microstructure at different substrate temperatures (a) $T=400$ K, (b) $T=500$ K, (c) $T=600$ K, and (d) $T=700$ K at $t=5000$ s; $W=1$ layer/s and $L=100$.

roughness square at different substrate temperatures do not follow the same power law as at $T=300$ K; see Fig. 16. For example, the roughness square increases almost linearly with respect to time at $T=600$ K at short times, which differs from the power law with an exponent of 0.5 at low temperatures. The different short-time dynamics at higher temperatures indicates crossover behavior of the kMC model. This crossover behavior is due to the competition of different processes at different growth conditions and may be described by other dynamic equations instead of the EW equation. At high temperatures, the high migration rate results in a dense film with little or no porosity, and thus, the current model can be approximated by a solid-on-solid model on a square lattice, of which the governing equations and the scaling behaviors have been intensively investigated (e.g., [26,27]). However, the triangular lattice model used in this work differs from the solid-on-slid model in several aspects even at the high temperature limit, e.g., the isotropy of the migration process. Such difference may result in deviation from EW behavior. Further study of the growth dynamics at higher temperatures will be the subject of future work.

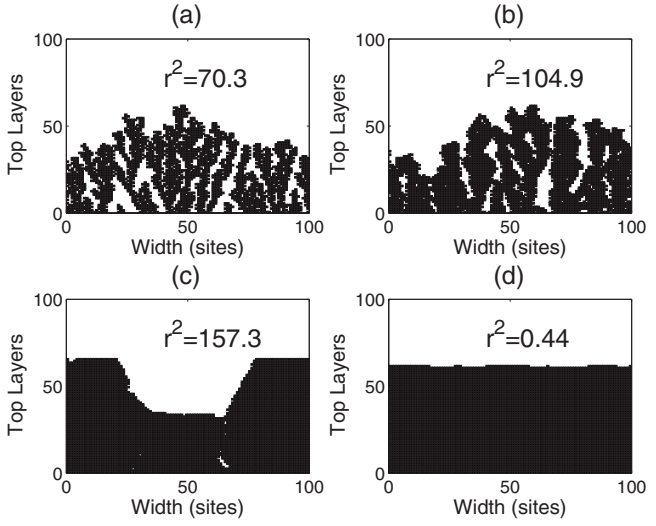

FIG. 15. Snapshots of film surface morphology (60 layers right below the top surface layer are shown) at different substrate temperatures (a) $T=400$ K, (b) $T=500$ K, (c) $T=600$ K, and (d) $T=700$ K at $t=5000$ s; $W=1$ layer/s and $L=100$.

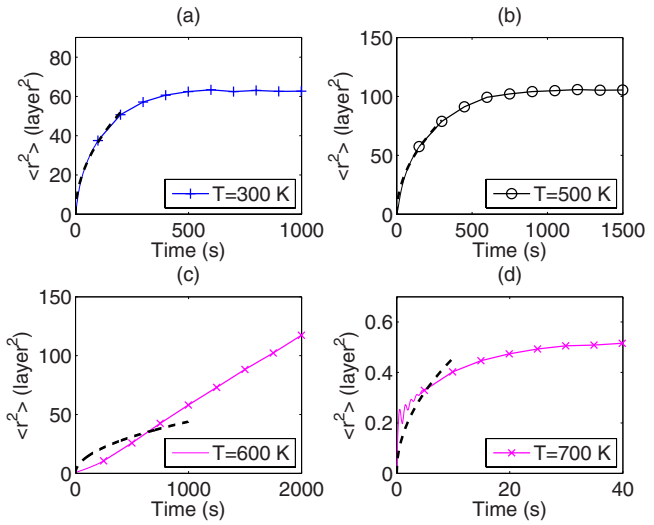

FIG. 16. (Color online) Profiles of the expected surface roughness square from kMC simulations (solid lines) and the fitted power-law time dependence with an exponent of 0.5 at short times ($\langle r^2\rangle = r_0\sqrt{t}$, dashed lines), at different substrate temperatures (a) $T=300$ K, (b) $T=500$ K, (c) $T=600$ K, and (d) $T=700$ K; $W=1$ layer/s and $L=100$.

C. Analytical results from the Edwards-Wilkinson equation

The EW-type equation, which is a second-order stochastic PDE, can be used to describe the surface height evolution in many microscopic processes that involve a thermal balance between adsorption (deposition) and migration (diffusion) [10,17]. The dynamic scaling properties of the EW equation have been investigated previously by other researchers [28]. In this section, the EW equation subject to periodic boundary conditions (this choice is made for consistency with the boundary conditions used in the kMC simulation) is solved analytically using modal decomposition. The theoretical results from the analytical solution of the EW equation corroborate the computational findings described above on the dependence of the dynamics of $\langle r^2\rangle$ on the lattice size and on the deposition time at low substrate temperature ($T \leq 500$ K). This corroboration supports the use of the EW equation with appropriate parameters as a continuum model to describe the surface height evolution in the thin film growth process under consideration [9,29]. Using the notation $h(x,t)$ to describe the surface height in the continuum case, the EW equation takes the following form [10]:

$$\frac{\partial h}{\partial t} = r_h + \nu \frac{\partial^2 h}{\partial x^2} + \xi(x,t), \tag{4}$$

subject to the following periodic boundary conditions:

$$h(-L_0,t)=h(L_0,t), \quad \frac{\partial h}{\partial x}(-L_0,t)=\frac{\partial h}{\partial x}(L_0,t) \tag{5}$$

and the initial condition

$$h(x,0)=h_0(x), \tag{6}$$

where $x\in[-L_0,L_0]$ is the spatial coordinate, t is the time, r_h and ν are the model parameters, specifically, r_h is related to the average growth rate of film surface and ν is related to the effect of particle relaxation and migration, and $\xi(x,t)$ is a Gaussian white noise with the following expressions for its mean and covariance:

$$\langle \xi(x,t)\rangle = 0,$$

$$\langle \xi(x,t)\xi(x',t')\rangle = \sigma^2\delta(x-x')\delta(t-t'), \tag{7}$$

where $\langle\cdot\rangle$ denotes the mean value, σ^2 is a parameter which measures the intensity of the Gaussian white noise and $\delta(\cdot)$ denotes the standard Dirac delta function. The choice of the Gaussian white noise can be validated by the histogram of surface height at sufficiently large times, which follows closely a Gaussian probability distribution [9]. In Eq. (4), time t and the spatial coordinate x are treated as continuous variables. Thus, the EW equation is valid for large time and large lattice sizes.

To proceed with model parameter estimation, a stochastic ordinary differential equation (ODE) approximation of Eq. (4) is first derived using modal decomposition. Consider the eigenvalue problem of the linear operator of Eq. (4), which takes the form

$$\nu\frac{d^2\phi_n(x)}{dx^2}=\lambda_n\phi_n(x),$$

$$\phi_n(-L_0)=\phi_n(L_0), \quad \frac{d\phi_n}{dx}(-L_0)=\frac{d\phi_n}{dx}(L_0), \tag{8}$$

where λ_n denotes an eigenvalue and ϕ_n denotes an eigenfunction. A direct computation yields the eigenvalues, $\{0, -\nu\frac{\pi^2}{L_0^2}, -\nu\frac{\pi^2}{L_0^2}, -\nu\frac{4\pi^2}{L_0^2}, -\nu\frac{4\pi^2}{L_0^2},\ldots\}$, and the eigenfunctions, $\{\frac{1}{\sqrt{2L_0}}, \frac{1}{\sqrt{L_0}}\sin\frac{\pi x}{L_0}, \frac{1}{\sqrt{L_0}}\cos\frac{\pi x}{L_0}, \frac{1}{\sqrt{L_0}}\sin\frac{2\pi x}{L_0}, \frac{1}{\sqrt{L_0}}\cos\frac{2\pi x}{L_0},\ldots\}$. The set of eigenfunctions is orthonormal. Note that the eigenvalues are sorted as $\|\lambda_0\|\le\|\lambda_1\|\le\|\lambda_2\|\le\cdots$, and thus, for fixed $\nu<0$, $\lambda_0=0$, and $\lambda_n<0$, for $n=1,2,\ldots$. From the eigenvalue problem, it can be inferred that the eigenvalues have the following dependence on the domain size, L_0,

$$\lambda_n=O(L_0^{-2}), \quad n=1,2,\ldots,\infty. \tag{9}$$

The solution of Eq. (4) is then expanded in an infinite series in terms of the eigenfunctions of the operator of Eq. (8) as follows:

$$h(x,t)=\sum_{n=0}^{\infty}\alpha_n(t)\phi_n(x), \tag{10}$$

where $\alpha_n(t)$ are time-varying coefficients. Substituting the above expansion for the solution, $h(x,t)$, into Eq. (4) and taking the inner product with the adjoint eigenfunction [i.e., $\int_{-L_0}^{L_0}h(x,t)\phi_n(x)dx$, the adjoint eigenfunction is the same as $\phi_n(x)$], the following system of infinite stochastic ODEs is obtained:

$$\frac{d\alpha_n}{dt}=c_n+\lambda_n\alpha_n+\xi_\alpha^n(t), \quad n=0,1,\ldots,\infty, \tag{11}$$

where

$$\alpha_n=\int_{-L_0}^{L_0}h(x,t)\phi_n(x)dx, \quad n=0,1,\ldots,\infty,$$

$$c_n=\int_{-L_0}^{L_0}r_h\phi_n(x)dx, \quad n=0,1,\ldots,\infty. \tag{12}$$

Due to the properties of the eigenfunctions, c_0 is a constant and c_n is zero, for $n=1,2,\ldots,\infty$, and

$$\xi_\alpha^n(t)=\int_{-L_0}^{L_0}\xi(x,t)\phi_n(x)dx, \quad n=0,1,\ldots,\infty. \tag{13}$$

with the following stochastic characteristics: $\langle\xi_\alpha^n(t)\rangle=0$ and $\langle\xi_\alpha^n(t)\xi_\alpha^n(t')\rangle=\sigma^2\delta(t-t')$.

Since the stochastic ODE system is linear, the analytical solution of state variance can be obtained from a direct computation as follows:

$$\langle\alpha_n^2(t)\rangle=-\frac{\sigma^2}{2\lambda_n}+\left(\langle\alpha_n^2(t_0)\rangle+\frac{\sigma^2}{2\lambda_n}\right)e^{2\lambda_n(t-t_0)}, \quad n=1,2,\ldots,\infty, \tag{14}$$

where $\langle\alpha_n^2(t_0)\rangle$ is the state variance at time t_0.

Similar to the lattice case, the surface roughness is the standard deviation of the surface height from its average value and is defined as follows:

$$r(t)=\sqrt{\frac{1}{2L_0}\int_{-L_0}^{L_0}[h(x,t)-\bar{h}(t)]^2dx}, \tag{15}$$

where $\bar{h}(t)=\frac{1}{2L_0}\int_{-L_0}^{L_0}h(x,t)dx$ is the average surface height.

According to Eq. (10), we have $\bar{h}(t)=\alpha_0(t)\psi_0$. Therefore, $\langle r^2(t)\rangle$ can be rewritten in terms of the state variance as follows:

$$\begin{aligned}\langle r^2(t)\rangle &= \frac{1}{2L_0}\left\langle\int_{-L_0}^{L_0}[h(x,t)-\bar{h}(t)]^2dx\right\rangle\\ &= \frac{1}{2L_0}\left\langle\int_{-L_0}^{L_0}\left[\sum_{i=0}^{\infty}\alpha_i(t)\phi_i(x)-\alpha_0(t)\phi_0\right]^2dx\right\rangle\\ &= \frac{1}{2L_0}\left\langle\int_{-L_0}^{L_0}\sum_{i=1}^{\infty}\alpha_i^2(t)\phi_i^2(x)dx\right\rangle\\ &= \frac{1}{2L_0}\left\langle\sum_{i=1}^{\infty}\alpha_i^2(t)\right\rangle\\ &= \frac{1}{2L_0}\sum_{i=1}^{\infty}\langle\alpha_i^2(t)\rangle.\end{aligned} \tag{16}$$

Equation (16) provides a direct link between the state variance of the infinite stochastic ODEs of Eq. (11) and the

expected surface roughness of the thin film. Note that the model parameter r_h does not appear in the expression of surface roughness since the zeroth state, α_0, is canceled out in the computation of the surface roughness.

The steady-state value of the expected surface roughness is obtained at the large-time limit ($t \to \infty$) of Eq. (16) and using Eqs. (14) and (9) we obtain:

$$\langle r^2 \rangle_{ss} = \langle r^2(\infty) \rangle = \frac{1}{2L_0} \sum_{i=1}^{\infty} \langle \alpha_i^2(\infty) \rangle = -\frac{1}{2L_0} \sum_{i=1}^{\infty} \frac{\sigma^2}{2\lambda_n} = O(L_0). \tag{17}$$

From Eq. (17), the steady-state value of the expected surface roughness square depends linearly on the domain size, L_0. This linear dependence is consistent with the large-L numerical results in Sec. III A.

The dynamics of the evolution of surface roughness also has a strong dependence on the domain size. By substituting the eigenvalues and manipulating the solution of Eq. (14), it follows that

$$\langle \alpha_n^2(t) \rangle = -\frac{\sigma^2}{2\lambda_n} + \left(\langle \alpha_n^2(t_0) \rangle + \frac{\sigma^2}{2\lambda_n} \right) e^{-2\nu n^2 \pi^2 (t-t_0)/L_0^2},$$

$$n = 1, 2, \ldots, \infty. \tag{18}$$

It can be concluded from Eq. (18) that the dynamics of the surface roughness square scale quadratically with respect to the domain size.

The previous analytical results are consistent with the simulation results of Sec. III A. Hence, the EW equation is an appropriate stochastic PDE model that can be used in the modeling and control of film surface roughness of the thin film deposition process in question.

Remark 3. A typical ballistic deposition model can be described by the Kardar-Parisi-Zhang (KPZ) equation, which gives different scaling properties of the roughening surface from the EW equation [30]. However, the deposition model studied in this work is not a typical ballistic deposition model, e.g., the particles on the film are subject to migration process due to the thermal effect. Thus, the scaling properties of the triangular lattice model cannot be described accurately by the KPZ equation at low temperatures ($T \leq 500$ K). This conclusion can be verified by the computational findings in Sec. III A. The roughness square follows a power growth law dependence with an exponent of 0.5 with respect to time at short times and the saturation time of the roughness square depends quadratically on the lattice size, which, respectively, indicates $\beta = 1/4$ and $z = 2$ in the following scaling equation [20]:

$$\langle r^2 \rangle \approx L^{2\alpha} f(tL^{-z}),$$

$$\langle r^2 \rangle \sim \begin{cases} t^{2\beta}, & t \to 0 \\ L^{2\alpha}, & t \to \infty \end{cases}, \tag{19}$$

where α is the static scaling exponent, β is the growth exponent, z is the dynamical scaling exponent, and $\beta = \alpha/z$. The exponents of $z = 2$ and $\beta = 1/4$ of the triangular lattice model, computed from our simulations for $T \leq 500$ K, are not consistent with the KPZ equation, where $z = 3/2$ and $\beta = 1/3$ for the one-dimensional case [30].

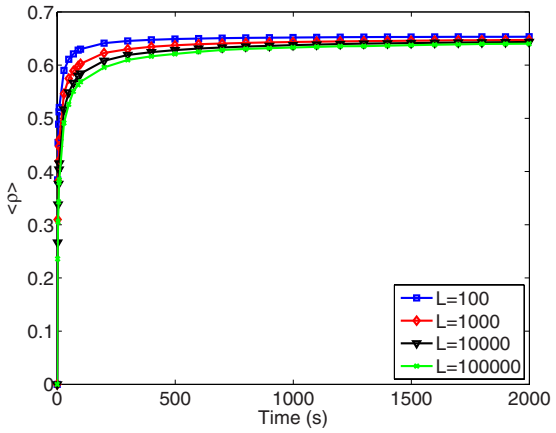

FIG. 17. (Color online) Profiles of the expected film SOR from kMC simulations with different lattice sizes; $W = 1$ layer/s and $T = 400$ K.

IV. LATTICE-SIZE DEPENDENCE OF FILM POROSITY

In this section, the dependence of film porosity (i.e., film SOR) on the lattice size at different substrate temperatures is investigated through kMC simulations. An integral model of film SOR is derived and is used to estimate the steady-state values.

A. Integral model of film site occupancy ratio evolution

Figure 17 shows the evolution profile of the expected film SOR at $W = 1$ layer/s and $T = 400$ K. Since the film SOR is a cumulative property, i.e., the denominator in the ratio increases with respect to time, the fluctuation of the film SOR decays to zero at large times [8]. Consequently, the required independent simulation runs to compute expected evolution profiles (especially for steady states at large times) can be much less than the necessary simulation runs for surface roughness. For a lattice size of 20, 1000 independent runs are sufficient to obtain accurate steady-state values. For larger lattice sizes, the fluctuations of film SOR further decrease due to the increased denominator in the ratio, and thus, fewer independent simulations are needed. Therefore, a wide range of lattice size (from 20 to 100 000) can be investigated for film SOR, as shown in Fig. 17. The specific numbers of independent simulation runs are listed in Table II.

From Fig. 17, it can be seen that the evolution profiles of the film SOR are similar to the ones of the surface roughness. The film SOR profiles increase from zero and reach steady-state values at sufficient large times. However, the steady-state values of the film SOR can be achieved within 2000 s only for small lattice sizes ($L < 100$). For a large lattice size, the evolution of film SOR slows down and requires a longer simulation time to reach steady state. To overcome these enormous computational requirements, an integral model can be derived to estimate the steady-state values of film SOR with simulation data from limited simulation times.

TABLE II. Number of simulation runs (film SOR) for different lattice sizes.

L	$T=400$ K	$T=500$ K
20	1000	1000
50	1000	1000
100	1000	1000
200	1000	1000
500	1000	1000
1000	1000	1000
2000	200	200
5000	100	100
10000	100	50
20000	100	50
50000	50	50
100000	20	20

In the integrands, a concept of instantaneous film SOR, ρ_d, is first introduced and is defined as the spatial derivative of the number of deposited particles in the growth direction as follows [29]:

$$\rho_d = \frac{dN}{d(HL)}. \tag{20}$$

According to the definition of the adsorption rate, W, in Sec. II A, the infinitesimal variation in deposited particles, dN, can be written as follows:

$$dN = WLdt. \tag{21}$$

Since the lattice size, L, is constant, the expression of the derivative of the deposited layers, dH, can be obtained in the following form:

$$dH = \frac{dN}{\rho_d L} = \frac{W}{\rho_d} dt. \tag{22}$$

With the definition of ρ of Eq. (3) and the expressions of dN and dH of Eqs. (21) and (22), the film SOR can be rewritten in an integral form as follows:

$$\rho(t) = \frac{N_0 + \int_{t_0}^{t} WLds}{\left(H_0 + \int_{t_0}^{t} \frac{W}{\rho_d} ds\right) L}, \tag{23}$$

where N_0 and H_0 denote the number of deposited particles and deposited layers at time t_0.

To simplify the integral form of film SOR in Eq. (23), it is necessary to investigate the time dependence of the integrands, i.e., the adsorption rate, W, and the instantaneous film SOR, ρ_d. In kMC simulations of the deposition process, W remains time-invariant. Figure 18 shows the evolution profile of ρ_d [obtained directly from the kMC simulation using Eq. (20)], which quickly approaches steady state and remains constant. From the evolution profile of ρ_d in Fig. 18, we infer that for sufficiently large times ($t \geq t_0$, where t_0 is the threshold of sufficiently large time), ρ_d can be approximated by its steady state value, ρ_d^{ss}. Using that $\rho_d \cong \rho_d^{ss}$, the integral form of film SOR of Eq. (23) can be simplified as follows:

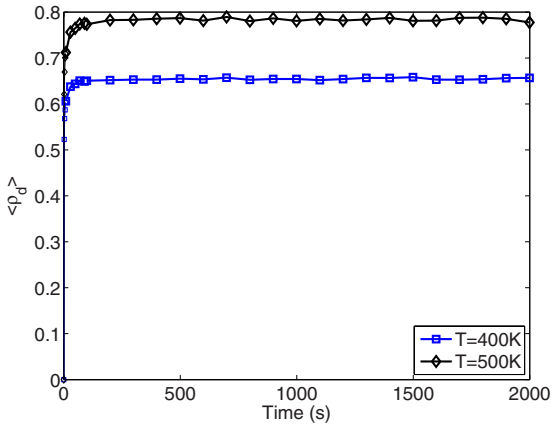

FIG. 18. (Color online) Profiles of the instantaneous film SOR from kMC simulations at different substrate temperatures, $T=400$ K and 500 K; $W=1$ layer/s and $L=100$.

$$\rho(t) = \frac{N_0 + WL(t - t_0)}{\left[H_0 + \frac{W}{\rho_d^{ss}}(t - t_0)\right] L}. \tag{24}$$

From Eq. (24), it follows that at large times, the film SOR approaches a steady-state value, ρ^{ss}, which equals the steady-state value of the instantaneous film SOR, ρ_d^{ss}. Equation (24) can be used to estimate $\rho(t)$ for large times (in particular, $t \geq 2000$ s) that cannot be accessed with the available computing power and compute ρ^{ss}. To achieve this, a least-squares method is used to estimate the steady-state value of ρ_d^{ss} by fitting Eq. (24) to $\rho(t)$ data at finite times (400 s $\leq t \leq 2000$ s) obtained from the kMC simulation. In the least-squares formulation, the threshold for sufficiently large times, $t_0=400$ s, is estimated from the evolution profile of ρ_d of Fig. 18. Subsequently, the evolution of $\rho(t)$ for $t \geq 2000$ s is computed via Eq. (24).

Figure 19 shows that the evolution profiles and the predicted profiles of film SOR are very close to each other. The agreement between the predictions and the kMC data indicates that the integral model of Eq. (24) can describe the evolution of film SOR at large times and provide reasonable estimates of the steady-state value of film SOR.

Figure 20 shows the steady-state values of film SOR, ρ^{ss}, for different lattice sizes at $T=400$ K and $W=1$ layer/s. Figure 20 also includes the values of film SOR at $t=1000$ s and $t=2000$ s. The error bars of the film SOR are calculated from 5 averages of evenly divided groups of all simulation runs. Since the steady-state values are estimates from the evolution profiles, no error bars are presented with ρ^{ss}. For small lattice sizes, ρ^{ss} is very close to the values of film SOR at 1000 and 2000 s, which indicates that the film SOR has reached its steady state. However, for large lattice sizes, the time $t=2000$ s is not long enough for the film SOR to approach its steady state. A weak dependence of the

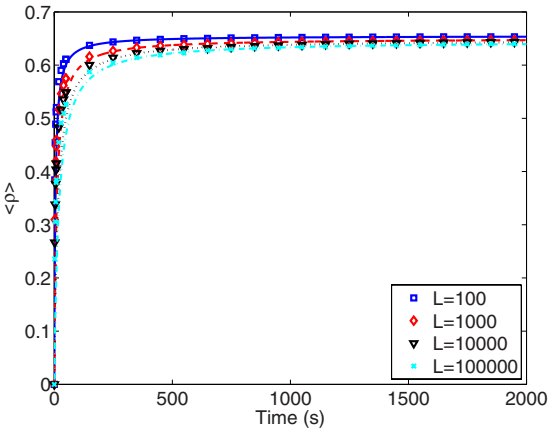

FIG. 19. (Color online) Profiles of the expected film SOR (discrete symbols) and of the predictions (continuous lines) from the integral model of Eq. (24); $W=1$ layer/s and $T=400$ K.

steady-state film SOR is observed in Fig. 20 (a logarithmic scale is used to show the large range of lattice sizes investigated in this work), where it can be seen that the steady-state value of the expected film SOR decays as the lattice size increases. The dynamics of film SOR also depends on the lattice size: large lattice sizes result in slow evolutions of the film SOR.

Remark 4. In previous work on modeling and control of film porosity, various dynamic models were derived to capture the evolution of film porosity, e.g., first-order ODE models [8,29]. These models were developed for the purpose of modeling and control of film porosity and its fluctuations. However, first-order ODE models are not suitable to estimate the steady-state values of film SOR. The film SOR is a cumulative property, which has different dynamics at small and large times and cannot be accurately represented by first-order ODE models for all times. On the contrary, the integral model of Eq. (24) is based on the steady-state approximation of the instantaneous film SOR at sufficiently large times, and thus, it can be used to better estimate the steady-state values of film SOR. It is important to note that the model of Eq. (24) cannot be used to describe the evolution of film SOR for

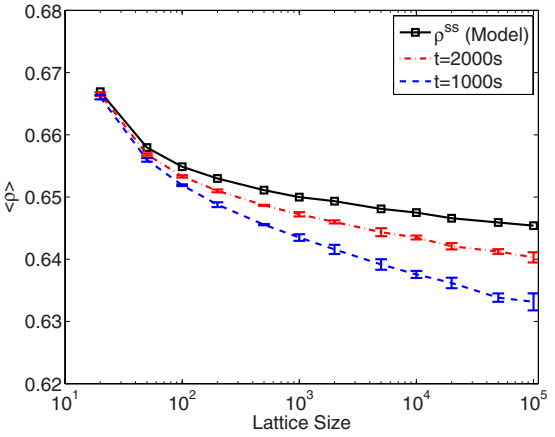

FIG. 20. (Color online) Profiles of the predicted steady-state values, the values at $t=1000$ s and $t=2000$ s of the expected film SOR for different lattice sizes; $W=1$ layer/s and $T=400$ K.

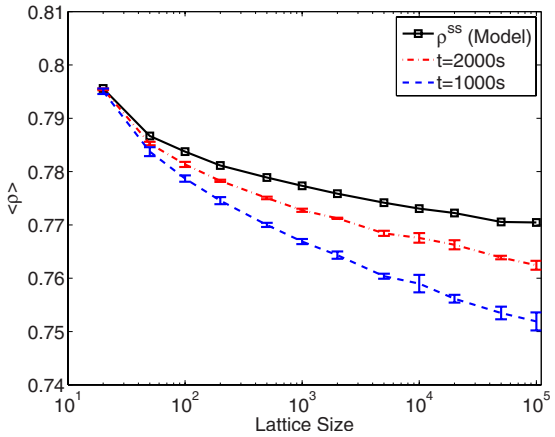

FIG. 21. (Color online) Profiles of the predicted steady-state values, the values at $t=1000$ s and $t=2000$ s of the expected film SOR for different lattice sizes; $W=1$ layer/s and $T=500$ K.

all times; it is not appropriate for short times and may result in deviations of the predicted profiles from the kMC data, as shown in Fig. 19.

B. Influence of substrate temperature on film SOR

Process parameters also influence the evolution of film SOR. Simulations with different substrate temperatures, $T=400$ and 500 K, are carried out with an identical adsorption rate, $W=1$ layer/s. Figure 21 shows the dependence of steady-state values of expected film SOR on the lattice size at $T=500$ K and $W=1$ layer/s. Similar weak dependence is observed at both temperatures. It can also be seen that the steady-state film SOR is higher at 500 K, which corresponds to lower porosity.

The influence of substrate temperature on film SOR can be further observed in Fig. 22, which shows the evolution profiles of film SOR at different substrate temperatures. A lattice size of 100 sites is used in all simulations. The steady-state values can be estimated using the integral model derived in Sec. IV A. Figure 23 shows the model-predicted steady-state values of film SOR at different substrate tem-

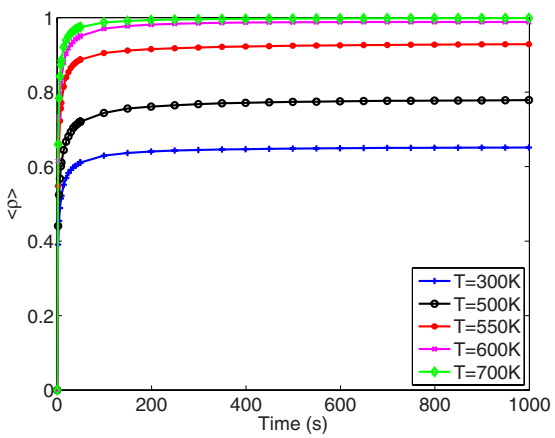

FIG. 22. (Color online) Profiles of the expected film SOR at different substrate temperatures; $W=1$ layer/s and $L=100$.

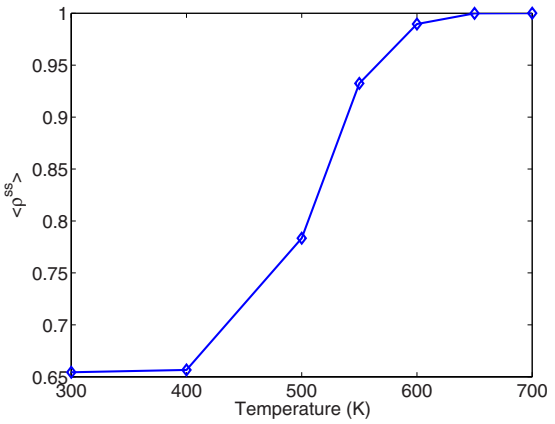

FIG. 23. (Color online) Dependence of the steady-state values of the expected film SOR on the substrate temperature; $W=1$ layer/s and $L=100$.

peratures. No error bars are presented in Fig. 23 since these values are model-predicted steady-state values. In Fig. 23, there are asymptotes at both low and high temperatures. When the substrate temperature is low, the film microstructure is mostly determined by the adsorption process due to the limited surface migration rates. However, at high temperatures, ρ^{ss} approaches unity since the film is fully packed due to the fact that particle migration is dominant. The influence of substrate temperature can be also seen in Fig. 14, where the increased temperature leads to a denser film with a lower porosity.

V. CONCLUSIONS

A thorough study of the dependence of film surface roughness and porosity on lattice size in a porous thin film deposition process was conducted. Specifically, a porous thin film deposition process which includes atom adsorption and migration was considered and was modeled via kMC simulations on a one-dimensional triangular lattice. Extensive numerical simulations were carried out to determine the variation in the film surface roughness and porosity with lattice size. For sufficiently large lattice size the steady-state value of the expected film porosity has a weak dependence on the lattice size and the steady-state value of the expected surface roughness square varies linearly with lattice size. A theoretical analysis based on stochastic PDE descriptions of film morphology was carried out to support and explain the computational findings.

ACKNOWLEDGMENTS

The authors are grateful to the Intel Higher Education Program, which provided the Linux cluster used in the simulations. Financial support from NSF, Grant No. CBET-0652131, is gratefully acknowledged.

[1] Y. Lou and P. D. Christofides, Ind. Eng. Chem. Res. **45**, 7177 (2006).
[2] Y. Lou and P. D. Christofides, Chem. Eng. Sci. **58**, 3115 (2003).
[3] P. D. Christofides, A. Armaou, Y. Lou, and A. Varshney, *Control and Optimization of Multiscale Process Systems* (Birkhäuser, Boston, 2008).
[4] S. W. Levine, J. R. Engstrom, and P. Clancy, Surf. Sci. **401**, 112 (1998).
[5] P. Zhang, X. Zheng, S. Wu, J. Liu, and D. He, Vacuum **72**, 405 (2004).
[6] S. W. Levine and P. Clancy, Modell. Simul. Mater. Sci. Eng. **8**, 751 (2000).
[7] L. Wang and P. Clancy, Surf. Sci. **473**, 25 (2001).
[8] G. Hu, G. Orkoulas, and P. D. Christofides, Chem. Eng. Sci. **64**, 3668 (2009).
[9] G. Hu, G. Orkoulas, and P. D. Christofides, Ind. Eng. Chem. Res. **48**, 6690 (2009).
[10] S. F. Edwards and D. R. Wilkinson, Proc. R. Soc. London, Ser. A **381**, 17 (1982).
[11] J. Villain, J. Phys. I **1**, 19 (1991).
[12] R. Cuerno, H. A. Makse, S. Tomassone, S. T. Harrington, and H. E. Stanley, Phys. Rev. Lett. **75**, 4464 (1995).
[13] C. A. Haselwandter and D. D. Vvedensky, Phys. Rev. B **74**, 121408 (2006).
[14] C. A. Haselwandter and D. D. Vvedensky, Phys. Rev. E **76**, 041115 (2007).
[15] C. A. Haselwandter and D. D. Vvedensky, Phys. Rev. E **77**, 061129 (2008).
[16] G. Hu, Y. Lou, and P. D. Christofides, Chem. Eng. Sci. **63**, 4531 (2008).
[17] F. Family, J. Phys. A **19**, L441 (1986).
[18] M. Kardar, Physica A **281**, 295 (2000).
[19] A.-L. Barabási and H. E. Stanley, *Fractal Concepts in Surface Growth* (Cambridge University Press, New York, 1995).
[20] F. D. A. Aarão Reis, Phys. Rev. E **63**, 056116 (2001).
[21] C. A. Haselwandter and D. D. Vvedensky, Phys. Rev. E **73**, 040101(R) (2006).
[22] Y. G. Yang, R. A. Johnson, and H. N. Wadley, Acta Mater. **45**, 1455 (1997).
[23] D. G. Vlachos, L. D. Schmidt, and R. Aris, Phys. Rev. B **47**, 4896 (1993).
[24] P. B. Maksym, Semicond. Sci. Technol. **3**, 594 (1988).
[25] S. Keršulis and V. Mitin, Mater. Sci. Eng., B **29**, 34 (1995).
[26] M. Kotrla and P. Šmilauer, Phys. Rev. B **53**, 13777 (1996).
[27] C. A. Haselwandter and D. D. Vvedensky, EPL **77**, 38004 (2007).
[28] T. Nattermann and L.-H. Tang, Phys. Rev. A **45**, 7156 (1992).
[29] G. Hu, G. Orkoulas, and P. D. Christofides, Chem. Eng. Sci. **64**, 3903 (2009).
[30] M. Kardar, G. Parisi, and Y. C. Zhang, Phys. Rev. Lett. **56**, 889 (1986).